Eur Biophys J (2007) 36:743–752
DOI 10.1007/s00249-007-0163-1

ORIGINAL PAPER

A statistical light scattering approach to separating fast and slow dynamics

Application to a model system

Jennifer Barthès · Donatella Bulone · Mauro Manno · Vincenzo Martorana · Pier Luigi San Biagio

Received: 15 January 2007 / Revised: 19 March 2007 / Accepted: 20 March 2007 / Published online: 13 April 2007

Abstract Light scattering is a powerful technique to study the structural and dynamical properties of biomolecular systems or other soft materials such as polymeric solutions and blends or gels. An important application of this technique is the study of the kinetics of formation of supramolecular structures. However, in such cases, the system under study is rapidly changing, and consequently the integration time for each measurement is limited. In order to overcome this difficulty, a statistical approach has been developed based on the analysis of the scattered light intensity distribution (Manno et al. 2006, 2004). Indeed the intensity distribution depends upon the ratio between the integration time of each measurement and the coherence time of scattered radiation. This method has been applied to protein aggregation (Manno et al. 2006) and to sol-gel transition (Manno et al. 2004), to obtain information on the heterogeneity of morphological and dynamical features during such processes. In the present work, we accurately test the validity of this approach by analyzing the statistical properties of the light scattered by a model system: a solution of polystyrene spherical macromolecules of different sizes. Each molecular size is related to a given diffusion coefficient and to a given coherence time of the scattered intensity. The effect of changing the experimental integration time is systematically investigated. A mixture of particles of two different sizes is also analyzed to test the validity and robustness of the model based on the convolution of a gaussian with an exponential distribution.

Keywords Fast kinetics · Fluctuation analysis · Light scattering (Exp and Theory)

Abbreviations

DLS	Dynamic light scattering
LALS	Large angle light scattering
PLS	Polystyrene sphere

Introduction

Light scattering is a powerful experimental technique to obtain structural and dynamical information on molecular solutions, gels, or other soft materials (Brown 1993). Indeed, the absolute magnitude of scattered intensity is related to the mass and to the structural properties of the studied sample. Also, the statistical properties of scattered radiation mirror the dynamical properties of the sample itself. This is the basis of the well-known photon correlation spectroscopy (Berne and Pecora 1976). In the best-studied case, the diffusion of a macromolecule in solution yields an exponential decay in the correlation function of the scattered electric field. The decay or relaxation time is inversely proportional to the diffusion coefficient of the scattering molecules, and hence directly proportional to their size. When the solution is made from several macromolecular species with different sizes the intensity autocorrelation functions may be fit by a regularization method, which gives the distribution of correlation times and therefore of molecular sizes (Štěpánek 1993).

Proceedings of the XVIII Congress of the Italian Society of Pure and Applied Biophysics (SIBPA), Palermo, Sicily, September 2006.

J. Barthès · D. Bulone · M. Manno · V. Martorana (✉) · P. L. San Biagio
Institute of Biophysics (section of Palermo),
Italian National Research Council,
via Ugo La Malfa, 153, 90146 Palermo, Italy
e-mail: vincenzo.martorana@pa.ibf.cnr.it

A particularly important application of scattering techniques is that of macromolecular solutions undergoing supramolecular self-assembly (Lomakin et al. 1999). In such a case, the system is intrinsically unstable and the time available for any measurements depends upon the rate of the aggregation kinetics. Thus, the measure of intensity correlation may be time consuming and not promptly available. In some recent papers (Manno et al. 2006, 2007), the kinetics of protein aggregation has been studied by the analysis of the statistical properties of scattered intensity. By using an appropriate model for the intensity distribution function, the contribution to scattering intensity due to slowly-diffusing, large size aggregates has been filtered out. The core of this model is the ratio between the integration time T_I of each measure of scattered intensity and the coherence time τ_c of the scattered radiation which is due to a particular macromolecular species or aggregate (Manno et al. 2004).

Indeed, the instantaneous scattered intensity $I = |E(t)|^2$ is exponentially distributed, since the electric field $E(t)$ scattered by a large number of objects is a complex gaussian variable (Pusey 1977). However, in typical scattering experiments the total measured intensity I_{TI} is time-averaged over a given time window: $I_{T_I} = \int_0^{T_I} |E(t)|^2 \mathrm{d}t$. Thus, when the integration time T_I is not larger than the coherence time τ_c of the scattered field, the intensity distribution is substantially equivalent to that of an instantaneous intensity. When T_I is much larger than τ_c, which is the most typical case for diffusing molecules, the intensity distribution tends to a gaussian distribution. In the other intermediate cases, the calculation of the distribution of the integrated intensity is less straightforward (Goodman 2000). Moreover, in the currently available devices the intensity is collected as photon counting, so that each distribution should be transformed via a Poisson distribution function (Goodman 2000).

In the previous work (Manno et al. 2006, 2007), the scattered field has been considered as the sum of two contributions. The first one is a fast fluctuating field due to small size objects with a coherence time τ_F much smaller than the integration time T_I. The second one is a slowly decaying field due to large size objects with a coherence time τ_S larger or at least not smaller than T_I. Up to the second order coherence, the intensity distribution is the convolution of a gaussian and an exponential distribution. The method has been successfully applied to protein aggregation kinetics (Manno et al. 2006, 2007), as well as to gelation kinetics (Manno et al. 2004).

In the present work such statistical approach to light-scattering measurements is applied to a simple model system, which is made from an aqueous solution of freely diffusing, non-interacting polystyrene spherical particles. First, we accurately study the non trivial properties of the distribution of the integrated intensity by changing the integration time. Therefore, we extend such a study to a mixture of particles with two sizes, and two correlation times. This allows us to test the validity of the model based on the convolution of a gaussian and an exponential distribution. We show that this model is ideally suited to reveal the presence of non-gaussian noise in any time series of integrated-intensity. This noise is partially related to slow processes and to large size diffusing objects. The absolute scale is of course dictated by the integration time. Here, the meaning of the non-gaussian noise is discussed and correctly addressed.

Materials and methods

LALS measurements

Large angle light scattering measurements are performed with a Brookhaven BI200-SM goniometer, using a diode pumped solid-state laser (Suwtech LDC-2500), at $\lambda_0 =$ 532 nm, at a scattering angle of 90°. The temperature has been kept to 25°C. A counter/timer board, National Instruments PCI-6602, allows to count photons detected by the photomultiplier with a temporal resolution of 25 ns (Magatti and Ferri 2002). The maximum data exchange bandwidth between PC memory and counter board limits the minimum sample time T_s to 2 μs. Our measurements, done with $T_s = 5$ μs, were performed by using a homemade Labview program. Raw data are written as binary files to a compressed filesystem to spare disk space (10 min–120 MB). The Labview program allows to monitor the count rate during the measurement, while the analysis is performed after the completion of data acquisition.

Samples preparation

Polystyrene spheres (PLS) with diameters 0.057 ± 0.008, 0.25 ± 0.02 and 2.09 ± 0.09 μm were purchased from Polysciences (Germany). Concentrations of each species were chosen to get approximately the same level of average scattered intensity and to avoid multiple scattering and particle–particle interactions. We used a density-matched solvent (48% H_2O, 52% D_2O) to avoid precipitation of the larger PLS. Concentrations are 13.3 μg/ml for the smaller beads (PLS1), 2 μg/ml for the spheres of intermediate size (PLS2), and 5 μg/ml for the larger beads (PLS3). A mixture (PLSm) of half volume of PLS1 and a half of PLS3 was also prepared. The dispersions were filtered directly into a cylindrical cuvette using Millex filter 0.22 μm for PLS1 and Sartorius filter 0.8 μm for PLS2. With the only exception of PLS1 we have observed very slow fluctuations of the photon count rate (with typical periods ranging from

10 s to few minutes). We noticed that the oscillation period could be increased by reducing the power of the incident radiation. To minimize the influence of this effect we decreased the incident power for a final count rate of ca. 15 kcount/s.

Computational methods

The correlation functions of the intensity are calculated using a C program that mimics the functioning of a logarithmic hardware correlator (Schätzel 1993), and allows the user to choose the number and the spacing of the delay times. The program implements the symmetric normalization of the correlation function (Schätzel 1993) that consists in dividing the correlation (average of intensity products) by the product of the averages of direct intensity and delayed intensity. As the input intensity can vary slowly this normalization improves the accuracy of the results.

The scattered intensity distributions at increasing integration time $T_I = 2^j T_s$, with $j = 0,1$ ... are computed by using a simple C code. We study integration times T_I ranging from 5 μs up to 1 second for measurements lasting ca. 600 s. The code adjusts the bin size of each histogram so as to keep the signal over noise ratio roughly constant. The first ten moments and cumulants are also concurrently computed.

On the statistics of time integrated scattered intensity

Here we recall some theoretical results on the distribution of time integrated scattered light intensity. In the case of a large number of identical, non interacting scatterers, subject to Brownian motion, the scattered electric field $E(t)$ measured at a chosen wave vector is a complex gaussian variable characterized by a single coherence time τ_F and the corresponding instantaneous intensity $I = |E(t)|^2$ is exponentially distributed with average $\bar{I}$ (Goodman 2000). The photomultipliers usually employed in light scattering instruments measure, during a time T_I, an average number of events $\bar{n}$ which is proportional to the product of the integration time by the time-integrated intensity

$$I(T_I) = \frac{1}{T_I} \int_{-T_I/2}^{T_I/2} |E(t')|^2 \mathrm{d}t' \tag{1}$$

when $T_I << \tau_F$ and for usual count rates, the distribution of the scattered intensity in terms of photocounts, $P(n)$, is a Poisson distribution. For values of T_I comparable to τ_F an approximate description of $P(n)$ can be given in terms of a Poisson-transformed gamma distribution (Goodman 2000)

$$P(n) = \frac{\Gamma(\mathscr{M}+n)\alpha^n}{\Gamma(\mathscr{M})\Gamma(n+1)[1+\alpha]^{\mathscr{M}+n}} \tag{2}$$

where $\Gamma(x)$ is the gamma function. For larger T_I values the effect of the discreteness of the detection process becomes negligible, and the distribution can be approximated by a gamma distribution:

$$P(n) = \frac{n^{\mathscr{M}-1}}{\Gamma(\mathscr{M})\alpha^{\mathscr{M}}} \exp(-n/\alpha). \tag{3}$$

The parameter α in (2) and (3) can be expressed as $\alpha = \bar{n}/\mathscr{M}$, where $\mathscr{M}$ is the number of coherence cells of the incoming radiation that influences the number of detected photons. In the special case of a lorentzian spectrum it is possible to calculate the value of $\mathscr{M}$ as (Goodman 2000)

$$\mathscr{M}_L(T_I,\tau_F) = \gamma \left\{ [\exp(-2T_I/\tau_F) + 2T_I/\tau_F - 1] \frac{2}{(2T_I/\tau_F)^2} \right\}^{-1} \tag{4}$$

where $\gamma > 1$ is introduced to take into account the effect of spatial averaging over different coherence areas due to the finite aperture of the detector. It is straigthforward to extend this result to the case of two lorentzian components, characterized by coherence times τ_F and τ_s:

$$\mathscr{M}(\tau_F,\tau_S) = \left\{ \frac{A^2}{\mathscr{M}_L(T_I,\tau_F)} + \frac{(1-A)^2}{\mathscr{M}_L(T_I,\tau_S)} + \frac{A(1-A)}{\mathscr{M}_L[T_I, \tau_F\tau_S/(\tau_F+\tau_S)]} \right\}^{-1} \tag{5}$$

where A represents the fraction of scattered light with coherence time τ_F.

An independent estimate of $\mathscr{M}$ can be obtained from the second cumulant of the photon counts statistics (Goodman 2000):

$$\widehat{\kappa}_2 = \frac{\overline{n^2} - \bar{n}^2}{\bar{n}^2} = \frac{1}{\bar{n}} + \frac{1}{\mathscr{M}} \tag{6}$$

Now let us focus on the special case of a two-component system with well- separated timescales ($\tau_F << T_I << \tau_S$) and let us neglect, for simplicity, the effect of the detection process on the statistics. It was shown by Pusey and collaborators that the distribution becomes (Pusey and van Megen 1989; Joosten et al. 1990):

$$P(I) = \mathrm{H}(I - \bar{I}_F)\ \exp\left[-\left(I - \bar{I}_F\right)/\bar{I}_S\right]/\ \bar{I}_S$$

with H(x) being the Heaviside function and $\bar{I}_F$ and $\bar{I}_S$ being the fast fluctuating and quasi-static components of the intensity, respectively. The result has been shown to hold in the case of a strong chemical gel (Joosten et al. 1990). It is common to study samples where the fast and slow process timescales are not so distant. In particular, during a kinetics, the separation between the timescales is evolving and it is sometimes an interesting result by itself. We have recently shown that it is possible to give a closed analytical expression for the distribution of the integrated intensity that is correct to the first order in $1/N = \tau_F/T_I$. We followed the same approach of Pusey and van Megen (1989), assuming that the scattered field E is the sum of a fast-fluctuating field E_F due to small-size objects with an average intensity $\bar{I}_F$, and a coherence time $\tau_F < T_I$, and a slowly decaying field E_S due to large-size slowly diffusing objects, with an average intensity $\bar{I}_S$, and a coherence time $\tau_S > T_I$. The total time-integrated intensity is given by the sum of these two fields over a time interval T_I as in (1). The study of the distribution cumulants gives:

$$\begin{aligned}
\kappa_1 &= \bar{I}_S + \bar{I}_F \\
\kappa_2 &= \bar{I}_S{}^2 + \frac{4}{N}\bar{I}_S\bar{I}_F + \frac{1}{N}\bar{I}_F^2 + O\left(N^{-2}\right) \\
\kappa_{i\geq 3} &= (i-1)!\left\{\bar{I}_S^i + \frac{2i}{N}\bar{I}_S^{i-1}\bar{I}_F + O\left(N^{-2}\right)\right\}
\end{aligned} \tag{7}$$

Since in the case of a sum of two statistically independent processes, the sum of their cumulants is equal to the cumulants of the sum (van Kampen 1992) we derived from (7) that the integrated intensity I can be interpreted as the sum of two statistically independent contributions: an exponentially distributed slow contribution with average $\bar{I}_{NG} = \bar{I}_S + 2\bar{I}_F/N$ and a gaussian-distributed fast contribution with average $\bar{I}_G = \bar{I}_F - 2\bar{I}_F/N$ and variance $\sigma^2 = \bar{I}_G^2/N$.

The expression for the intensity distribution function, that we will call gauss-exp in the following, is thus the convolution of a gaussian with an exponential function:

$$\begin{aligned}
P(I_{T_I}) = \bar{I}_{NG}^{-1}\exp\{-[I-\bar{I}_G]/\bar{I}_{NG}\} \\
\times\left[\mathrm{erf}\left(\frac{I}{\sigma\sqrt{2}} - \frac{\bar{I}_G\bar{I}_{NG}+\sigma^2}{\bar{I}_{NG}\sigma\sqrt{2}}\right)\right. \\
\left.+\,\mathrm{erf}\left(\frac{\bar{I}_G\bar{I}_{NG}+\sigma^2}{\bar{I}_{NG}\sigma\sqrt{2}}\right)\right]\frac{1}{2}\exp\left(\frac{\sigma^2}{2\bar{I}_{NG}^2}\right)C
\end{aligned} \tag{8}$$

where $\mathrm{erf}(x) = 2/\sqrt{\pi}\int_0^x e^{-t^2}\mathrm{d}t$ is the error function, and $C \approx 1$ is a normalization constant: $C = \frac{1}{2}\left[1 + \mathrm{erf}\left(\frac{\bar{I}_G}{\sigma\sqrt{2}}\right)\right]$.

Results and discussion

As mentioned in the Introduction we have applied the method of integrated intensity distribution analysis to monitor the appearance and growth of long decay times both in a gelling system (Manno et al. 2004) and in aggregating protein solutions (Manno et al. 2006, 2007).

In Fig. 1 we show the data of the kinetics of recombinant human insulin heated in acidic solution (pH 1.6 at 60°C). The aggregation leads to an overall increase of the scattered intensity, but also to an asymmetric broadening of the normalized distributions. Empirically this broadening is caused by the presence of lifetimes of the order of, or longer than, T_I. The distributions have been fitted to (8) with a good agreement. In this case the integration time T_I is set equal to 1 s so that only large objects (>100 μm) are expected to contribute to the quasi static scattered field. The estimate of the fraction of the fast fluctuating intensity was used in two recent papers (Manno et al. 2006, 2007) as a way of filtering out the contribution to the scattering due to very large objects. This, in turn, allowed us to uncover the physics of the aggregation mechanism of the smaller protein oligomers. In a system as complicated as the aggregating protein solution it is however difficult to establish quantitatively the resolution power gained through the analysis based on (8). Since such

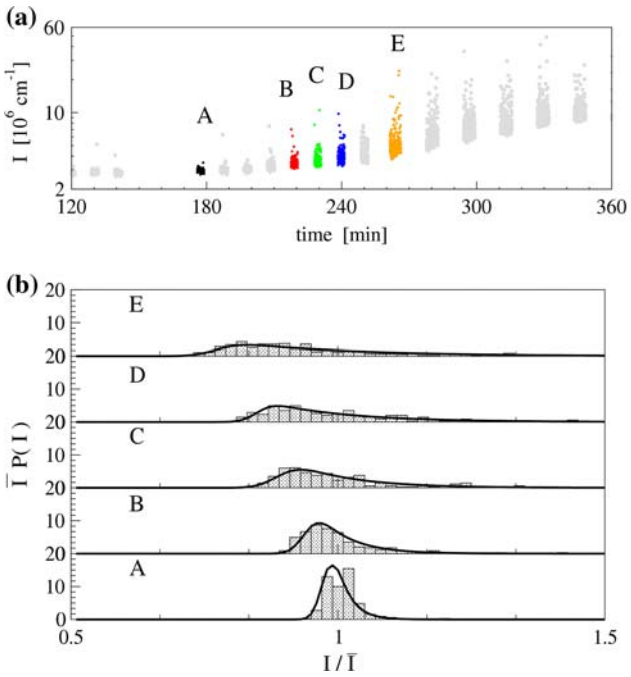

Fig. 1 (**a**) Scattered intensity distributions at different times of the aggregation kinetics. Data are fitted to Eq. 8 (*solid lines*). (**b**) Temporal evolution of 90° scattered intensity. Time intervals and distributions are related by matching upper-cases (A, B, C, D, E)

systems are inherently polydisperse and unstable, we now apply the same analysis to a much more simpler system, where just one or two characteristic times are important, i.e., dispersions of PLS spheres in aqueous solvent.

The result of a standard DLS measurement of the intensity correlation function is shown in Fig. 2 for PLS1, PLS2, PLS3 and PLSm. The data are fitted to the expression

$$g^{(2)}(\tau) - 1 = \beta^2(\exp(-\tau/\tau_0) + b)^2 \tag{9}$$

in the case of ''pure'' dispersions, and

$$g^{(2)}(\tau) - 1 = \beta^2[a\exp(-\tau/\tau_1) + (1 - a - b)\exp(-\tau/\tau_2) + b]^2 \tag{10}$$

in the case of the mixture. The parameters of the fitting are shown in Table 1 for the four dispersions. The hydrodynamic radii are in good agreement with the nominal radii. Polydispersity, as estimated from cumulant analysis, is ca. 4% for PLS2 and PLS3, and 10% for PLS1, while the baseline b is of the order of 4% with respect to the total amplitude. The τ_i of the single species PLS1, PLS2, PLS3, will be considered as the reference characteristic times in the following analysis.

The photon count distributions have been calculated for the different systems at increasing integration time. In Fig. 3 some distributions relative to PLS1 are shown. As T_I increases the distribution changes its shape from a Poisson-like distribution to a gaussian distribution, passing through a gamma distribution with increasing $\mathscr{M}$. Actually, at our experimental count rate, the *instantaneous* intensity is influenced by the Poisson noise so that a Poisson-transformed gamma distribution (also known as negative binomial distribution), (2), must be used to describe the histograms. For larger T_I a simple gamma distribution can be used to fit the histograms. At the largest T_I/τ_1 ratio (bottom row) the distribution can hardly be distinguished from a gaussian. The fitting of data in Fig. 3, shown as continuous lines, are good for extreme values of the ratio T_I/τ_1, and less satisfying for intermediate values of T_I/τ_1, where a more rigorous approach (Slepian 1958) would be beneficial. Nonetheless, the quality of the fitting is sufficient, in our opinion, to capture the change in the number of coherence time intervals $\mathscr{M}$ with increasing T_I.

This is confirmed by results in Fig. 4, where we plot the parameter $\mathscr{M}$ obtained by fitting the integrated intensity distributions for systems PLS1/2/3 to (2) and (3), versus the ratio between the integration time and the characteristic time of the scatterer as obtained from Table 1.

The data of PLS1 in Fig. 4 can be fitted satisfactorily to (4), i.e., a single lorentzian spectrum is sufficient to describe the dependence of $\mathscr{M}$ on the integration time. Surprisingly, an additional timescale must be introduced to interpret the data of PLS2 and PLS3. In fact the data tend to saturate for $T_I/\tau_i > 100$, suggesting the influence of a very long characteristic time. Thus we added a second lorentzian spectrum to the expression 4 and fitted the data to (5). The longer characteristic time is not well defined but, in any case, more than a thousand times larger than the smaller one. We can thus take the limit of (5) for $\tau_S \to \infty$, obtaining

$$\mathscr{M}'_L = \mathscr{M}_L / \left[A + (\tau_F/T_I)\,(1 - A)^2\,\gamma^{-1}\right] \tag{11}$$

In Table 2 we report the fitting parameters obtained using the above equation. We note that the presence of an infinite correlation time should show up as a baseline in the correlation functions of Fig. 2. The amplitudes of the baseline shown in Table 1 are of the same order of the value of the parameter (A–1) of (11). We also note that an apparently negligible baseline in $g^{(2)}$ heavily affects $\mathscr{M}$ at large T_I. For T_I/τ_i <1 The data points tend to settle around a value which

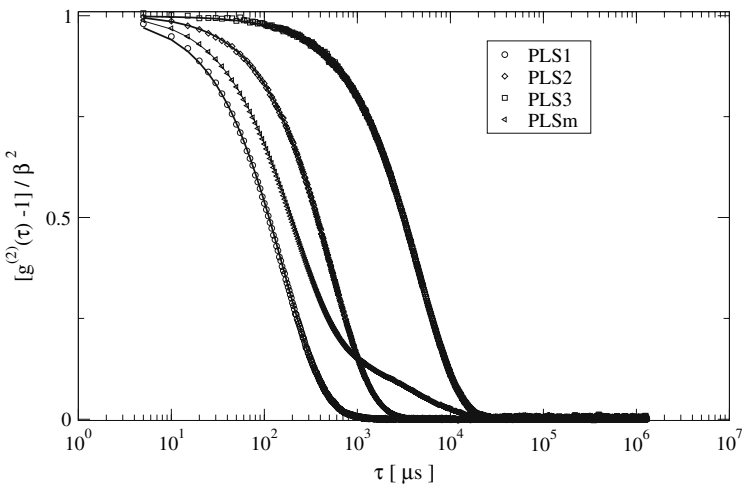

Fig. 2 Plots of $[g^{(2)}(\tau)–1]/\beta^2$ where $g^{(2)}(\tau)$ is the normalized time-averaged intensity correlation function. PLS1 (*circle*), PLS2 (*diamond*) and PLS3 (*square*) are fitted to (9) (*continuous lines*) while PLS1+PLS3 mixture (*left triangle*) is fitted to (10) (*continuous line*)

Table 1 Fitting parameters of correlation functions of PLS1, PLS2, PLS3 and the mixture PLSm

System	β	τ_1 (μs)	τ_2 (μs)	b	a	$2R_h$ (nm) exptl.
PLS1	0.74	328	–	0.001		75.2
PLS2	0.80	1,024	–	0.020		234
PLS3	0.70	8,630	–	0.027		1,963
PLSm	0.78	288	6,560	0.08	0.58	66.0 1492

The hydrodynamic radius R_h has been obtained from the Einstein relation $R_h = (k_B T q^2 \tau)/(6\ \pi\eta)$ where η is the viscosity of the solvent, k_B is the Boltzmann constant and q is wave vector

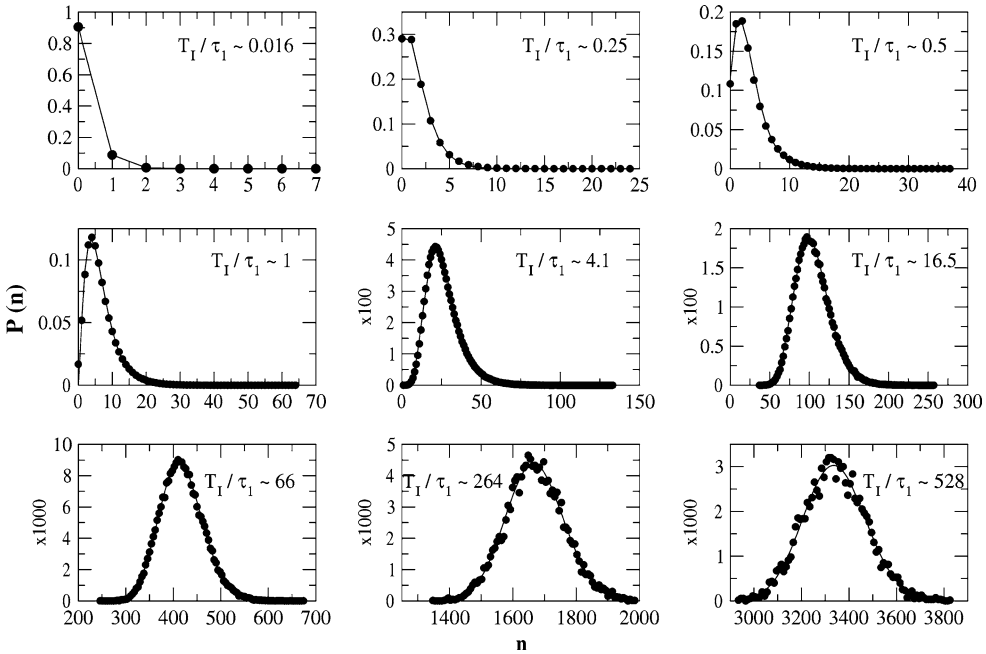

Fig. 3 Scattered photon counts histograms in the case of pure dispersion PLS1, at different integration times T_I. Histograms are fitted to Poisson-transformed gamma distribution (2) for $T_I/\tau_i < 1$, elsewhere to gamma distribution (3)

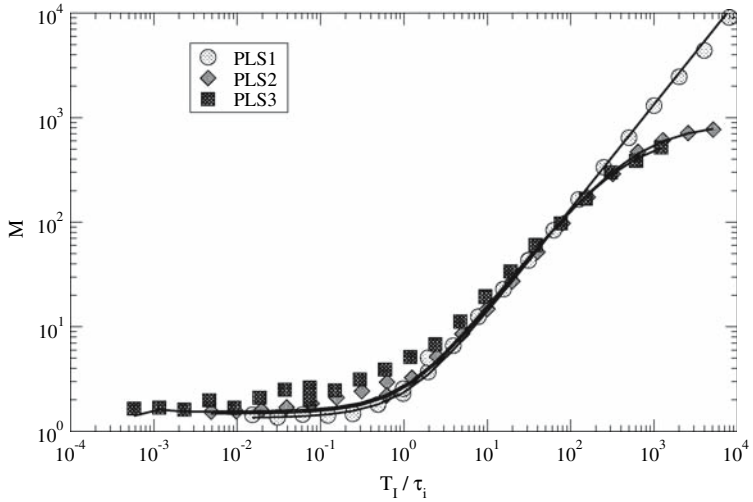

Fig. 4 Parameter $\mathscr{M}$ obtained from gamma distribution fits of histograms as described for Fig. 3. The three single dispersions PLS1 (*circle*), PLS2 (*diamond*), PLS3 (*square*) are fitted to (11) with parameters in Table 2

is definitely larger than 1. This is expected since, even for very small integration times, the value of $\mathscr{M}$ reflects the spatial averaging over different coherence areas (Goodman 2000) due to the finite area of the detector + optics.

Instead of pretending to know the shape of the photon count distribution of the integrated intensity, one can measure the cumulants straight from the count history. The case of the normalized second cumulant is illustrated in

Table 2 Fitting parameters of $\mathscr{M}$ for PLS1/2/3

System	γ	A-1
PLS1	1.34	0
PLS2	1.41	0.04
PLS3	1.47	0.05

Fig. 5. We recall that the second cumulant is strictly related to $\mathscr{M}$ (see 6). Substituting (4) in (6) and using the γ values of the fitting in Fig. 4 one obtains the lines in Fig. 5. Since we are taking into account a single lorentzian component the agreement between the theoretical function and the data points is good only up to $T_I/\tau_i \sim 100$. Note that the data for PLS1 show a curvature for $T_I/\tau_i > 10^4$, a range where the histograms are too noisy to be usable.

We now want to check whether it is possible and what it means to fit the histograms of photon counts described above, to (8), that was introduced to study systems where processes with fast and slow timescales coexist. In the PLS dispersions a single characteristic time is present and thus when $T_I \geq \tau$ we expect to find a small value of $\bar{I}_S/\bar{I}$, since on the scale of T_I the PLS diffusion represents a fast process and no slower scatterers are present. First of all we have checked that the quality of the fit to (8) is acceptable at least in the range $T_I \geq 10\ \tau$ where the approximation, on which the distribution is based, holds. As shown in Fig. 6 the quality of the fitting is comparable to that obtained using the gamma distribution. Actually the gauss-exp distribution works quite well (much better than the gamma distribution) at fitting the exponential tail of the histograms (data not shown). We can exclude that such tails be artifacts since the theoretical distributions for exponentially correlated intensity do show such tails for $I/\bar{I} > 2$, as we have checked by numerical computation (Slepian 1958). The parameter N of Eq. 8 is closely related to $\mathscr{M}$ as shown in the inset of Fig. 6. The values of N are systematically larger than $\mathscr{M}$, in particular at small values of $\mathscr{M}$.

In Fig. 7 are shown the values of $x_F = \bar{I}_F/\bar{I}$ for the three PLS dispersions.

Since we are looking at the time range $T_I > 10\ \tau_i$, we would expect to find $x_F \sim 1$. As a matter of fact, we find that the data start from values around 0.85 and increase slowly toward the unity. We associate this unwanted effect to the persistence of an exponential tail in the photocount histograms for T_I values up to 100 τ_i. Such tail is actually well fitted by the gauss-exp distribution and thus wrongly attributed to a slow process.

It is interesting to note that the curves can be superimposed by rescaling the time axis by the respective correlation times, as shown in the inset of Fig. 7. Moreover it is possible to find a master curve using a power law $x_F = 1-\{1 + 2.4\ (T_I/\tau_i)\}^{-0.6}$. In summary the dependence of x_F on the time is smooth and not steep.

In the case of the mixture of polystyrene particles of two different sizes, we can fully examine the behavior of the distribution as well as the fitting parameter obtained by using (8). In Fig. 8 nine histograms are shown with T_I ranging from $0.5\tau_F$ to $125\tau_F$–23 τ_S, where τ_F and τ_S are the correlation times relative to the small and large PLS spheres, respectively. Note that the dynamic range is quite large (up to 10^5) and that the gauss-exp distribution (continuous line in Fig. 8) is capable of fitting quite well. No matter what the value of T_I is, the histogram features a clear exponential tail which increases its slope at increasing T_I. On the basis of the analysis of the correlation function (10), we would expect to find $x_F \sim 0$ for $T_I < \tau_F$, $x_F \sim 0.6$ for $\tau_F > T_I > \tau_S$, and $x_F \sim 1$ for $T_I > \tau_S$. Such ideal values are indicated in Fig. 9 with a dashed line. The data points, instead, varies from 0.4 to 0.8 and are very close to the expected value only for T_I values between 10^3 and 2×10^3 μ s. It happens that this range is the optimal one in terms of distance both from the fast and the slow characteristic times. We observe again the same underestimation

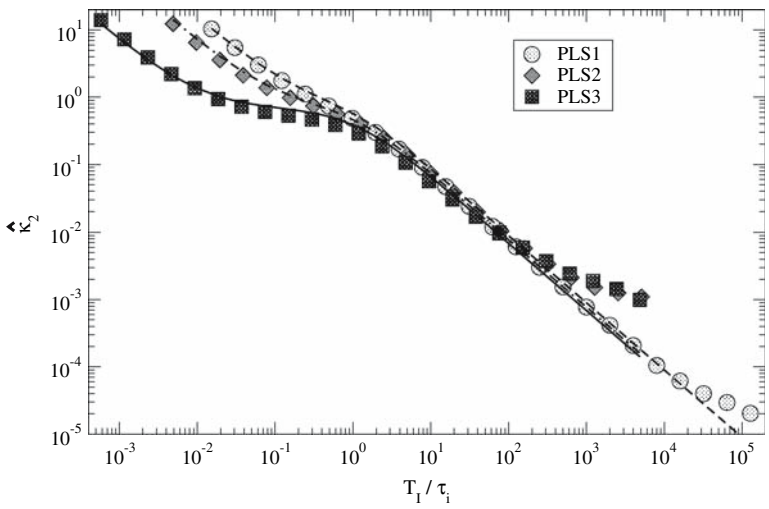

Fig. 5 Normalized second cumulant of photon counts versus T_I/τ_i. The three sets of data, PLS1 (*circle*), PLS2 (*diamond*) and PLS3 (*square*), are fitted to (6) with values for γ equal to those in Table 2

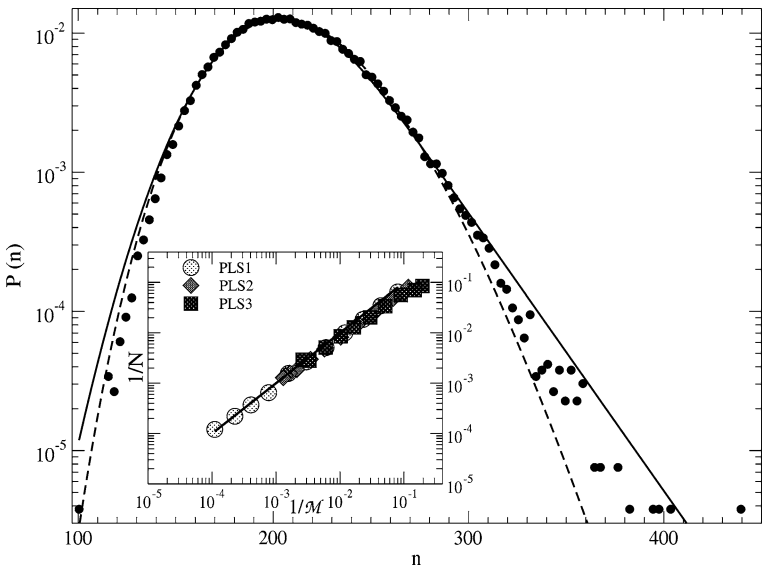

Fig. 6 Comparison of the fitting with the gamma and the gauss-exp distributions. For sample PLS1 (*filled circle*) at $T_I/\tau_1 = 34$, gamma distribution fit is shown as a dashed line and gauss-exp distribution as a continuous line. In the *inset*: parameter N obtained by fitting the histograms with the gaus-exp distribution (8), versus parameter $\mathscr{M}$, obtained from gamma distribution fit (2 and 3)

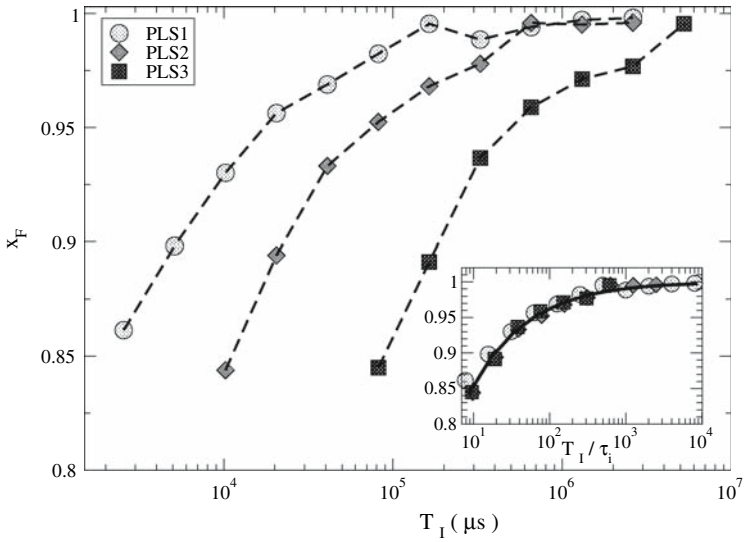

Fig. 7 Fraction of the *fast* contribution to scattered light, with respect to T_I, as estimated from fittings to gauss-exp distribution for PLS1 (*circle*), PLS2 (*diamond*), PLS3 (*square*). In the *inset*: Fast contribution fraction for PLS1/2/3 dispersions with respect to T_I/τ_i (*same symbols*)

of x_F for $T_I >> \tau_S$ described above, and the absence of clear slope changes in correspondence to the two relevant correlation times. From what we have seen we can predict that the non ideal behavior of x_F could be less pronounced in the case of a large timescale separation between the fast and the slow processes. In the present case the maximum relative error in determining the contribution of diffusive processes with a correlation time lower than the integration time is of 20%. Indeed, the integration time T_I is not a sharp threshold between fast and slow processes. As we made it clear above, all processes which are ''slower'' than the integration time do not contribute to the ''fast'' fraction x_F. In addition, all processes which are ''faster'' than the integration time are included in the fast fraction to some extent with a power law dependence. Therefore, this approach provides a statistical filter for slow processes. Equivalently, this method is very useful to highlight the onset of non-gaussian noise during aggregation kinetics.

Conclusions

Light-scattering techniques are widely used in biophysics to determine structural and dynamic properties of solutions or gels of biomolecules. Robust and thoroughly tested analysis tools are nowadays available to get useful information out of the raw photocount history. However, in the case of fast kinetics involving the appearance of long characteristic times the standard tools could be inefficient. In such cases it is possible to perform the recently proposed (Manno et al. 2004) analysis of the integrated intensity distributions in terms of fast and slow processes, where fast

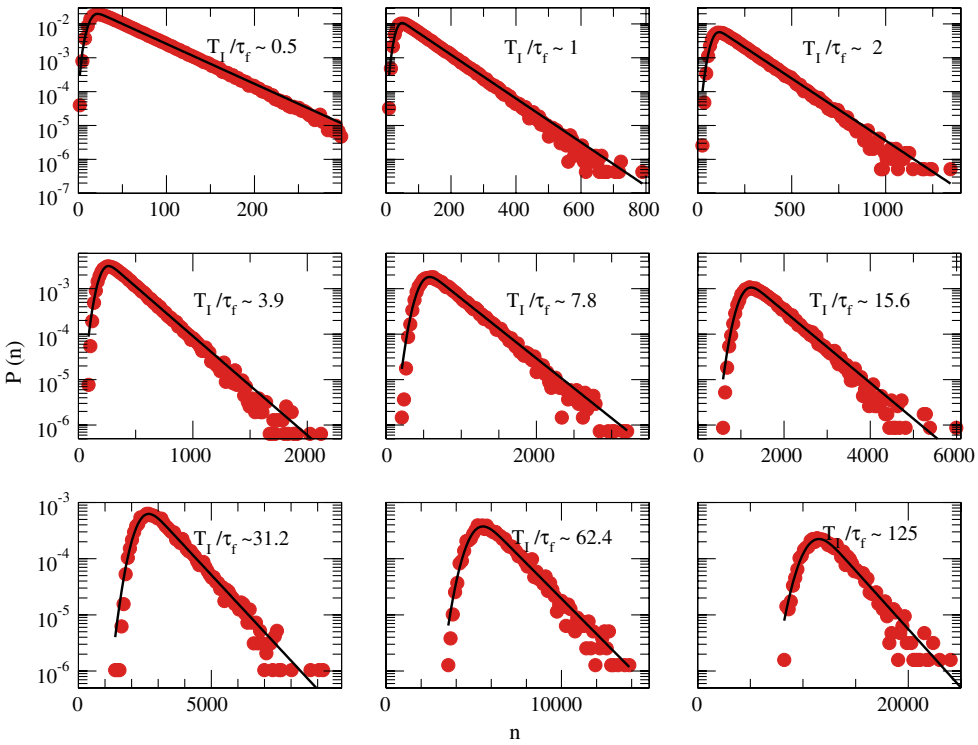

Fig. 8 Scattered photon counts histograms in the case of mixture dispersion PLS1 + PLS3, at different integration times T_I. Histograms are fitted to gauss-exp distribution (8)

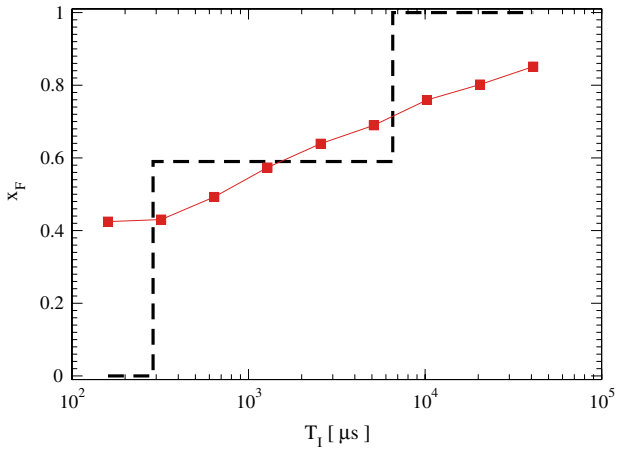

Fig. 9 Fraction of the *fast* contribution to scattered light as estimated from fitting in Fig. 7. The *dashed line* represents the stepwise, ideal behavior expected on the basis of the correlation function analysis

and slow are defined in terms of the integration time. This theoretical study proposes also an approximate distribution function that is a convolution of a gaussian and an exponential distribution (gauss-exp distribution).

We have here studied the effect of changing the latter in the case of a model system comprising simple PLS spheres of different sizes. We have shown that the histograms of photocounts can be fitted to a Poisson- transformed gamma distribution, or to a simple gamma distribution, depending on the average number of counts during the integration time. We obtained the parameter $\mathscr{M}$ which varies as expected for scattered light whose correlation is decaying exponentially. Strong deviations at large T_I can be explained as the effect of very slow fluctuations of scattered intensity and are in agreement with the amplitude of the baselines of the respective field correlation functions.

The histograms of photocounts have also been fitted to the gauss-exp distribution for integration times larger than the PLS characteristic time at the given wave vector. The results for the different PLS can be superimposed by scaling the times with the respective characteristic times. The fraction of fast-fluctuating intensity x_F is not univocally ascribed to diffusional processes which are faster than the integration time T_I. Other processes with a characteristic time τ_F larger than T_I contribute to x_F, with a power law dependence upon the ratio τ_F/T_I. As a rule of thumb, we may consider that processes with $\tau_F > 100\, T_I$ give a negligible contribution to x_F (see Fig. 7). This unsharp separation of slow and fast processes may be explained by the presence of an exponential tail in the histograms which is captured by the gauss-exp distribution as a sign of a slow process, stealing to the fast fraction. The exponential tail appears to be a relic of the instantaneous intensity distribution and survives to relatively large integration times. The same effect is apparent in the case of a mixture of the two PLS spheres whose size (and correlation times) differ by a factor 23. Again the fraction of fast intensity starts from a low of 0.4 and reaches the expected value only

within an interval of integration times that is sufficiently far both from the fast and the slow processes.

The analysis of the photocount histograms with the gauss-exp distribution is capable of assigning the correct fraction of slow and fast scattered intensity even in the case of a timescale separation of ca. one order of magnitude. As it is clear from Fig. 7, a good estimate of x_F can be obtained only by a judicious choice of the integration time. We expect to find a more robust behavior for larger timescale separation.

Two additional effects can influence the efficiency and reliability of the statistical approach tested here. One is the poissonian character of the detection process that is most apparent at low count rate. For an integration time larger than a fraction of a second and for usual count rates this is not going to be a major problem. The second effect is due to the averaging of more than one coherence area at the detector. The net result of this effect will be an underestimation of the fraction of the slow component of the scattered light and should be taken into account when the β factor estimated from measurements of the correlation function is grossly less than one.

References

Berne BJ, Pecora R (1976) Dynamic light scattering. Wiley Interscience, New York

Brown W (1993) Dynamic light scattering: the method and some applications. Clarendon Press, Oxford

Goodman JW (2000) Statistical optics. Wiley, New York

Joosten JGH, Geladé ETF, Pusey PN (1990) Dynamic light scattering by nonergodic media: Brownian particles trapped in polyacrylamide gels. Phys Rev A 42:2161–2175

Lomakin A, Benedek GB, Teplow DB (1999) Kinetic analysis of amyloid fibril formation. Methods Enzymol 309:429–459

Magatti D, Ferri F (2002) 25 ns software correlator for photon and fluorescence correlation spectroscopy. Rev Sci Instr 74:1135–1144

Manno M, Bulone D, Martorana V, San Biagio PL (2004) Ergodic to non-ergodic transition monitored by scattered light intensity statistics. Physica A 341:40–54

Manno M, Craparo EF, Bulone D, Martorana V, San Biagio PL (2006) Kinetics of insulin aggregation: disentanglement of amyloid fibrillation from large-size cluster formation. Biophys J 90:4585–4591

Manno M, Craparo EF, Podestà A, Bulone D, Carrotta R, Martorana V, Tiana G, San Biagio PL (2007) Kinetics of different processes in human insulin amyloid formation. J Mol Biol 366:258–274

Pusey PN (1977) Statistical properties of scattered radiation. In: Cummings HZ, Pike ER (eds) Photon correlation spectroscopy and velocimetry. Plenum Press, New York

Pusey PN, van Megen W (1989) Dynamic light scattering by non-ergodic media. Physica A 157:705–741

Schätzel K (1993) Single-photon correlation techniques. In: Brown W (ed) Dynamic light scattering: the method and some applications. Clarendon Press, Oxford

Slepian D (1958) Fluctuations of random noise power. Bell Syst Tech J 37:163–184

Štěpánek P (1993) Data analysis in dynamic light scattering. In: Brown W (ed) Dynamic light scattering: the method and some applications. Clarendon Press, Oxford, pp 177–240

Van Kampen NG (1992) Stochastic processes in physics and chemistry. North-Holland, Amsterdam